

Direct numerical simulation benchmarks for the prediction of boundary layer bypass transition in the narrow sense

Xiaohua Wu

Royal Military College of Canada,

Carlos A. Gonzalez

Center for Turbulence Research, Stanford University,

Rahul Agrawal*

Center for Turbulence Research, Stanford University

(Dated: March 7, 2025)

We report a comprehensive set of direct numerical simulation benchmarks of bypass transition in the narrow sense with inlet freestream turbulent intensity levels 0.75%, 1.5%, 2.25%, 3.0% and 6.0%, respectively. Detailed descriptions of length scales and the rate of viscous dissipation are provided. We ask two key physical questions. First, how do the decay rates and length scales of freestream turbulence over a transitional and turbulent boundary layer compare to those in spatially developing isotropic turbulence without the wall? Second, what bypass mechanisms drive turbulent spot inception at the intermediate range of freestream turbulence intensity level? We find that the boundary-layer freestream turbulence decay and length scales evolve similarly to their spatially developing isotropic turbulence flow without the wall counterparts. We also present evidence of the coexistence of two turbulent spot inception mechanisms at the inlet FST level 2.25%: the long low-speed streak primary and secondary instabilities (only in lower inlet FST levels) and the self-amplifying process of oblique vortex filaments interacting with a Delta-shaped low-speed patch underneath (prevailing only in higher inlet FST levels).

I. INTRODUCTION

Predicting boundary-layer transition is essential in several industry applications, including over aircraft wings, compressors, and turbine blades. To this end, transition modeling remains an active area of research. A crucial step in developing such models is their evaluation over zero-pressure-gradient, smooth-walled, flat-plate boundary layer (ZPGSFPBL) under isotropic freestream turbulence (FST) with varying inlet intensity levels ($FSTI_{in}$). Wu [26] classified such flows as boundary-layer bypass transition in the narrow sense to distinguish them from bypass transition arising from other phenomena, including laminar separation bubbles, roughness elements, or very high-level FST.

Generally, the experiments of Roach [18] are used as a benchmark for calibrating and evaluating transition prediction models (see Westin and Henkes [24], Suzen and Huang [20], Menter et al. [14], Durbin [4], Ge et al. [6], Menter et al. [15]). Roach [18] reported wind-tunnel experiments in three conditions: case T3A with upstream turbulence intensity 3.5%, case T3B with upstream turbulence intensity 6.5%, and case T3A- with upstream turbulence intensity 0.8%. Interestingly, the skin friction coefficient, C_f , in these experiments collapses onto the Blasius laminar flow solution before breakdown. However, despite its varied usage, several notable drawbacks are still associated with this dataset. For instance, the C_f was estimated indirectly from momentum balance rather than from a measurement of the near-wall velocity gradient. Further, there are only a few recorded data points within the transition zone (C_f departs from the laminar solution and begins approaching the turbulent level), which is perhaps concerning as there is a wide gap in the freestream turbulence levels between cases T3A and T3B. Thus, there has been a need for additional reference datasets for use in transition model benchmarking and calibration.

In this spirit, from a computational standpoint, many direct numerical simulations (DNS) have been previously performed to study the transitioning boundary layer. We highlight the potential imperfections of such previous studies (see Fig. 1). For instance, in the previous DNSs of Brandt et al. [3], Jacobs and Durbin [8], Nagarajan et al. [16], the freestream turbulence decays much faster than the experiments [18]. A consequence of the overly rapid decay of

* Email: rahul29@stanford.edu

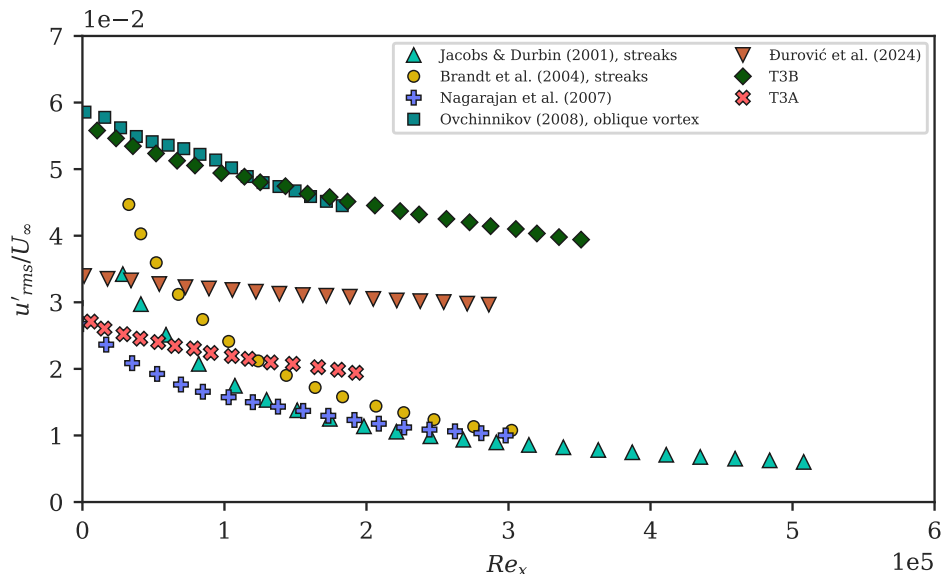


FIG. 1. Decay of freestream turbulence intensity in the previous studies on bypass transition in the narrow sense.

freestream turbulence is that the downstream stations (where the flow transitions) may experience lower turbulence intensities than desired. We briefly remark that previously, Ovchinnikov et al. [17] performed DNS of the transitioning boundary layer while including a leading edge and nearly reproduced the decay rates of T3B experimental case [18] for $FSTI_{in} \sim 6\%$. Ovchinnikov et al. [17] perform two simulations, one with a “full” domain, and one with a “symmetry plane” (about the midplane of the leading edge). In the laminar flow region, their C_f compares well with the Blasius solution in the full domain, but when the flow transitions, the C_f does not agree with the experiments [18]. In the half-domain case, the simulations don’t collapse onto the Blasius C_f in the laminar region. The spatial decay rate of the freestream turbulence in the DNS of Đurović et al. [23] also compares reasonably with Roach [18]. However, their C_f also does not collapse onto the Blasius solution before breakdown.

The present study contributes toward addressing these limitations. To the authors’ knowledge, the database herein covers a wider than currently published range of $FSTI_{in}$ conditions simulated under one computational framework. Further, we seek to answer two key physical questions: (i) how do the decay rates and length scales of freestream turbulence developing over a boundary layer compare to those in spatially developing isotropic turbulence? i.e., does the growth of the boundary layer affect the freestream turbulence? and (ii) what mechanisms drive turbulent spot inception at an intermediate range of $FSTI_{in}$?

Fundamentally, it is conjectured that the unsteady streamwise streaks dominate the boundary-layer bypass transition in the narrow sense, as supported by smoke flow visualizations, measurements of turbulence intensity profiles, and the non-modal theory on disturbance energy growth (the reader is referred to the works of Fransson and Shahinfar [5], Kendall [9], Matsubara and Alfredsson [12], Westin et al. [25]). Although smoke visualizations often reveal the existence of long streaks, and measurements of turbulence intensities and correlations often show agreement with algebraic growth theory, the intricate processes of Blasius boundary-layer breakdown and the inception of the one infant turbulent spot at the smallest possible streamwise Reynolds number for a given instant/cycle are difficult to capture in experiments, nor can these processes be definitively predicted by existing theory.

Wu et al. [27] observed turbulent spots in DNS of ZPGSFPBL bypass transition and tracked the inception process of the spots. Following this work, Alarcón et al. [2], Brandt et al. [3], Jacobs and Durbin [8], Nagarajan et al. [16], Ovchinnikov et al. [17], Đurović et al. [23], Wu [26], Wu et al. [28] have studied the flow over a transitioning boundary layer. Jacobs and Durbin [8] attempted to reproduce the T3A experiment with an $FSTI$ of 3.5%, and they found that infant spots arise from localized instabilities of low-speed streaks when the streaks interact with freestream turbulence. Brandt et al. [3] considered $FSTI$ values of 1.5%, 3%, and 4.7%, and reported that Blasius layer breakdown is related to local secondary instabilities of long low-speed streaks in the form of either the sinuous-type driven by the spanwise shear or the varicose-type by the wall-normal shear. Nagarajan et al. [16] used $FSTI$ values 3.5% and 4.5%, and included the leading edge in their compressible flow simulations. They found that at a

low level of FSTI, breakdown follows the streak-centered findings of Jacobs and Durbin [8] and Brandt et al. [3]. However, at a high level of FSTI, breakdown does not involve low-speed streaks. Ovchinnikov et al. [17] studied the $FSTI_{in} = 6.7\%$ case, similar to the T3B experiment to find that although low-speed streaks exist, infant turbulent spots are detected upstream of the region of the streaks, and that spot precursors are traced to spanwise structures. These structures reorient to become hairpin vortices, which break down into infant spots. On the contrary, Alarcón et al. [2] recently reported the convective evolution of the secondary instabilities of low-speed streaks using their DNS at $FSTI_{in} = 3.45\%$, also including a leading edge. They presented statistics supporting the dominance of streak secondary instabilities in the breakdown of the numerous low-speed streaks. However, their C_f notably differs from the Blasius solution in the early transition region.

Wu et al. [28] simulated the $FSTI_{in} = 3.0\%$ flow to find that the laminar boundary-layer breakdown is driven by a self-amplifying process of oblique vortex filaments interacting with a Δ -shaped low-speed patch underneath. The oblique vortex filaments (Λ vortex) flank the Δ patch. This process does not involve long, low-speed streaks. Sparse and chaotic low-speed streaks develop downstream of infant spots. These are consistent with the findings of Ovchinnikov et al. [17] at FSTI 6.7%. Further, Wu [26] found that at $FSTI_{in} = 1.5\%$, the laminar boundary layer breaks down when asymmetric inclined boundary-layer vortex filaments appear on one side of long low-speed streaks or when symmetric boundary-layer vortex filaments partially wrap the tail portion of a long low-speed streak (consistent with Brandt et al. [3]). The wavy appearance of streaks associated with the asymmetric inclined vortex filaments and symmetric vortex filaments are in line with the notions of ‘sinuous mode’ and ‘varicose mode’ of Swearingen and Blackwelder [21], respectively. Wu [26] suggested that the streak-instability spot inception mechanism may be relevant for $FSTI_{in}$ levels ranging from 0.5% to 2%, and the mechanism of self-amplifying oblique-vortex interaction with an underneath Δ -shaped low-speed patch may be more relevant for $FSTI_{in}$ levels ranging from 2.5% to 5%.

Given these findings, we seek to ask how the switch from the non-streak-dominated mechanism to the streak-dominated mechanism occurs with the reduction of $FSTI_{in}$. Alternatively, at some intermediate $FSTI_{in}$, would one breakdown mechanism dominate the other, or would the two mechanisms coexist in the same flow but at different instants/cycles? In this spirit, we also seek to answer if the developing boundary layer affects the freestream above it, which may, in turn, affect the transition process.

The rest of this work is organized as follows: Section II describes the computational method. Section III briefly discusses statistics of the DNS database including skin friction, and length, dissipation scales. Section IV assesses the decay of spatially evolving freestream turbulence with and without walls. Section V discusses the turbulent spot inception mechanisms, including at an intermediate level ($\approx 2.25\%$) of $FSTI_{in}$. Finally, concluding remarks are provided in Section VI.

II. COMPUTATIONAL METHOD

We perform five DNSs of boundary-layer bypass transition in the narrow sense and three additional DNSs on stand-alone spatially developing isotropic turbulent flow without a wall. The $FSTI_{in}$ levels for the five cases are 0.75% (denoted as WM075), 1.5% (denoted as WM150), 2.25% (denoted as WM225), 3.0% (denoted as WM300) and 6.0% (denoted as WM600), respectively (see Fig. 2 and Figs. 3(a) & (b)). The $FSTI_{in}$ levels of spatially-developing isotropic turbulence without the wall are 1.5% (denoted as SDIT150), 3.0% (denoted as SDIT300), and 6.0% (denoted as SDIT600), respectively (also see Fig. 3(c)).

The domain size, grid resolutions, inflow turbulence generation, boundary conditions, and numerical method for the WM-series DNSs are identical to those in Gonzalez et al. [7], Wu et al. [28] and skipped for brevity (as a marker for the sufficiency of the resolution, we briefly highlight that the spatial resolutions are smaller than 4η in wall parallel and wall-normal directions, including in the freestream for WM150 flow. Further, the temporal resolution is less than $\tau_\eta = (\nu/\varepsilon)^{1/2}$, or the local Kolmogorov time scale.)

Fig. 4 recapitulates some important parameters for the WM-series DNS. FST is introduced at the inlet over the wall-normal range $15\theta_{in} < y < L_{y,iso}$, where θ_{in} is the constant inlet boundary-layer momentum-thickness. Below and above this height, a uniform inflow (U_∞ , without fluctuations) and the mean Blasius velocity profile are fed, respectively. At the streamwise exit, domain height L_y is equivalent to 24.31, 9.05, 7.36, 7.24, and 6.66 local boundary-layer thickness δ_{exit} in WM075, WM150, WM225, WM300 and WM600, respectively. Given the substantial distance between the top surface and the wall, we hypothesize that the effect of the top boundary condition on boundary layer development is minimal. At the top of the computational domain, in the WM-series, we apply the following boundary

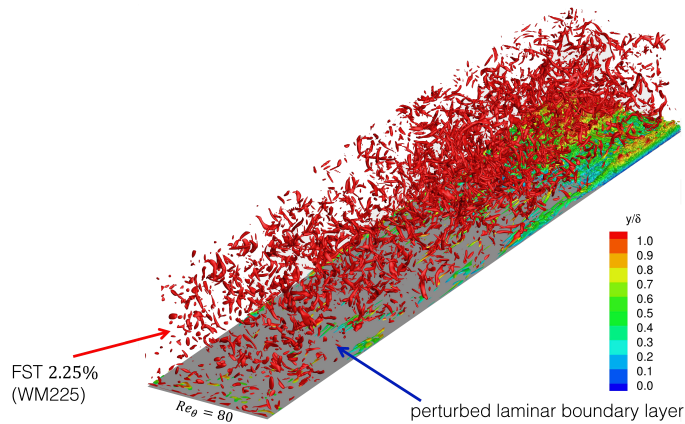


FIG. 2. Isosurfaces of swirling strength, as defined in Adrian [1], in WM225 over the transitional region.

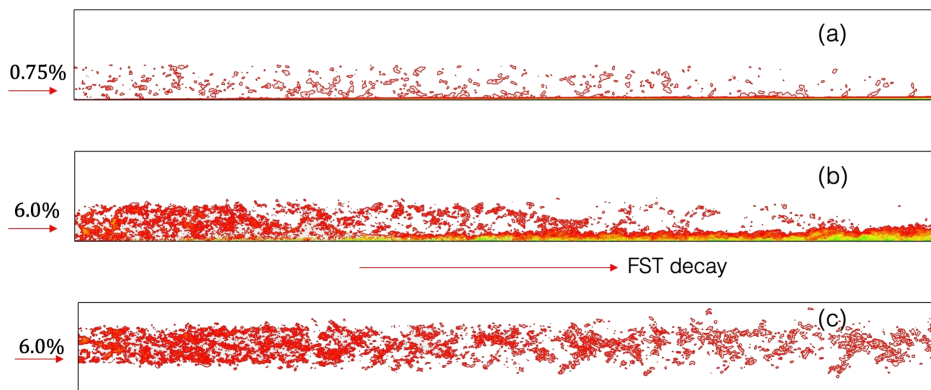


FIG. 3. Visualization of three DNS cases using contours of streamwise velocity u over a random xy -plane where blue and red colors indicate $u = 0$ and $u = U_\infty$, respectively. (a) WM075; (b) WM600; (c) SDIT600.

conditions: $v = v_{\text{blasius}}$, $\partial u / \partial y = \partial v / \partial x$, $\partial w / \partial y = \partial v / \partial z$.

For the SDIT-series DNSs, the domain size, inflow turbulence generation, and numerical method are the same as those in the WM-series (see Fig. 5). The inflow turbulence is positioned in the central region of the inlet. The grid resolution (provided in Fig. 5) is coarser than that in the WM series, as the absence of the wall reduces the demand for resolving the boundary-layer turbulence.

III. DNS BENCHMARKS FOR TRANSITION PREDICTION

A. Data accessibility

Here, we present the processed skin friction, shape factor, dissipation and evolution of integral and Taylor length scales from our DNSs. For the sake of brevity, other quantities such as boundary-layer thickness (δ), displacement thickness (δ^*), wall-pressure fluctuation ($p'_{w,rms}$), wall-shear stress fluctuation ($\tau'_{w,rms}$) are not presented. However, the streamwise growth of these data with the streamwise (Re_x), momentum thickness (Re_θ) or the friction-based (Re_τ) based Reynolds numbers are accessible from the Center for Turbulence Research website. Additionally, the database contains the wall-normal variations of the mean velocity (\bar{u}) and of turbulent stresses (u'_{rms} , v'_{rms} , w'_{rms} , $\overline{u'v'}$, p'_{rms} , where overbar indicates averaging), and total shear (τ) in outer units (y/δ) and viscous units (y^+) at selected streamwise stations covering the early, late and post-transition stages. The statistics were sampled on the fly at every time step over two convective flow-through times across the domain. The reader is referred to Gonzalez et al. [7], Wu et al. [28] for a discussion on the accuracy of the collected statistics.

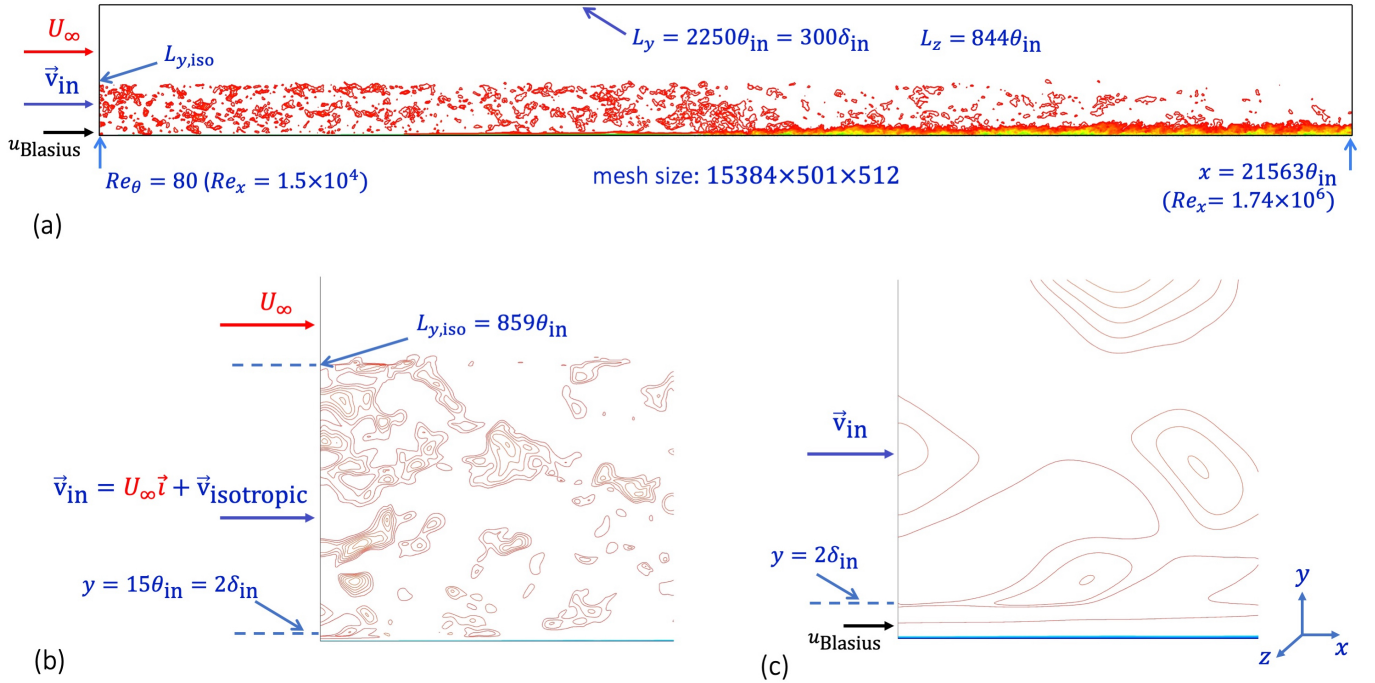


FIG. 4. Illustration of boundary layer DNS design using contours of streamwise velocity u over a random xy -plane where blue and red colors indicate $u = 0$ and $u = U_\infty$, respectively. (a) full view; (b) zoomed view near the inlet; (c) further zoomed view near the inlet.

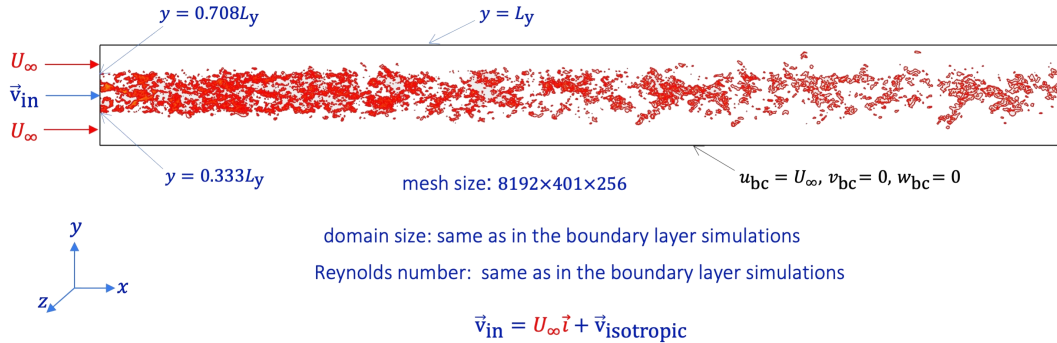


FIG. 5. Illustration of spatially-developing isotropic turbulence DNS design using contours of streamwise velocity u over a random xy -plane where blue and red color indicate low and higher values, respectively.

B. Skin-friction and shape factor

Fig. 6(a) presents the skin friction, C_f as a function of Re_x . All five DNSs show an extended domain range wherein the skin friction agrees well with the Blasius laminar flow solution. The departure from the Blasius solution is only visible slightly upstream of the minimum C_f location (a qualitative marker of early transition). The case WM075 does not complete the transition process across the present computational domain. The distribution of C_f against Re_θ is shown in Fig. 6(b). Slightly downstream of the peak plateau, C_f of WM225 flow collapses onto the WM300 profile. Similarly, the WM150 profile also collapses onto those of WM225 and WM300 after the peak, suggesting the downstream boundary layers after transition are turbulent with only minimal lingering transitional effects. The WM600 profile also nearly collapses with the other profiles, but the minor differences suggest that further higher freestream turbulence may cause substantial disturbances to the viscous sublayer of the turbulent boundary layer

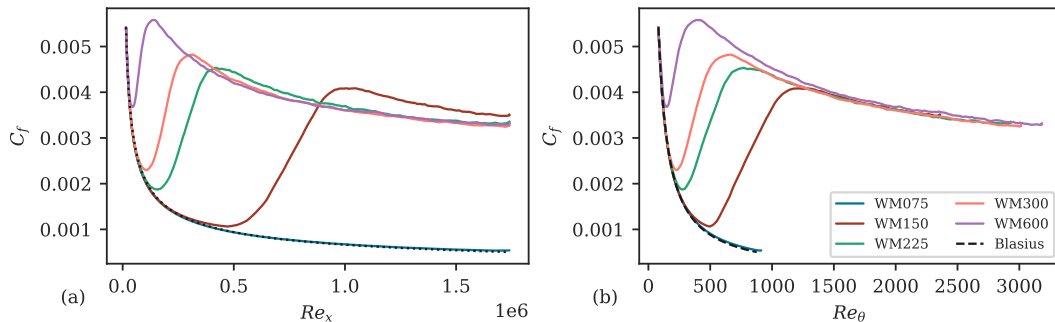


FIG. 6. Skin-friction coefficient as a function of (a) streamwise Reynolds number and (b) momentum-thickness Reynolds number in the five boundary layer DNS cases.

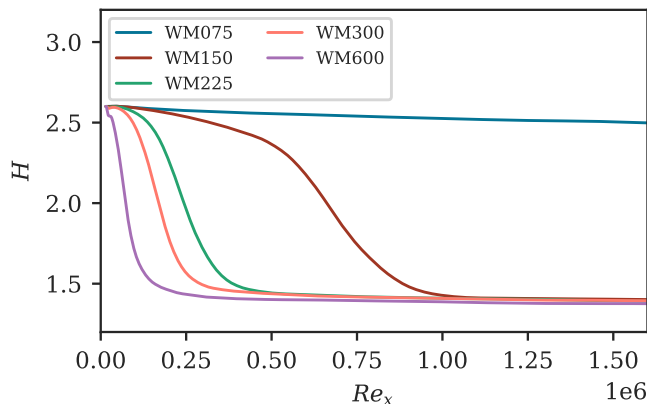


FIG. 7. Boundary-layer shape factor as a function of momentum-thickness Reynolds number in the five boundary layer DNS cases.

underneath (also see the boundary-layer shape factor H of WM600 in Fig. 7. The precipitous drop in the shape factor near the inlet for the WM600 case potentially implies a non-negligible disturbance on the boundary layer by the high freestream turbulence).

C. Length scales

Next, we present length scale information for the boundary layer DNSs. The rate of viscous dissipation ε appears in the definitions of Kolmogorov length scale $\eta = (\nu^3/\varepsilon)^{1/4}$ and the large-eddy scale $L = \text{TKE}^{3/2}/\varepsilon$, $\text{TKE} = (u'_{rms}{}^2 + v'_{rms}{}^2 + w'_{rms}{}^2)/2$. The dissipation rate, ε , is also used in several transition and turbulence models [10, 19].

Fig. 8 presents wall-normal profiles of $\varepsilon^+ = \varepsilon/(u_\tau^4/\nu)$ at four selected streamwise stations in WM150 and WM600. A narrow peak is observed at $y^+ \approx 60$, corresponding to $y \approx 1.9\delta$, at the $Re_\theta = 90$ station (which is slightly downstream of the inlet $Re_\theta = 80$ station). We believe this may be associated with the inflow boundary setup: FSTI_{in} is only imposed for $y > 2\delta$ (see Fig. 4). For both WM150 and WM600 cases (in Fig. 8), at stations downstream of the transition region, the dissipation profiles collapse well with the theoretical equation $\varepsilon^+ = 1/(\kappa y^+)$ where $\kappa = 0.421$ [13] which can be derived by assuming constant shear stress layer, logarithmic velocity profile, and the equilibrium between the production of TKE and ε (also see Tennekes and Lumley [22]).

Fig. 9(a) presents the wall-normal profiles of L/δ at eight selected streamwise stations in WM150 where δ is the local boundary layer thickness. The nearly constant values of L/δ for $y > 2.5\delta$ represent the freestream values. The sharp descent and rapid rise in the profile of $Re_\theta = 90$ near $1.8\delta < y < 2\delta$ is related to the peak of ε near $y \approx 1.9\delta$

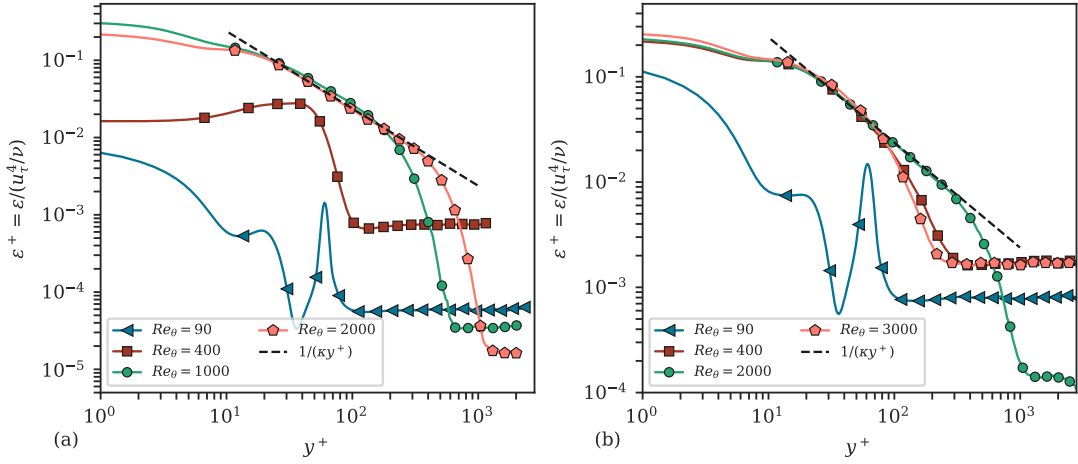


FIG. 8. Rate of viscous dissipation ε^+ profiles before, during, and after transition in (a) WM150 and (b) WM600.

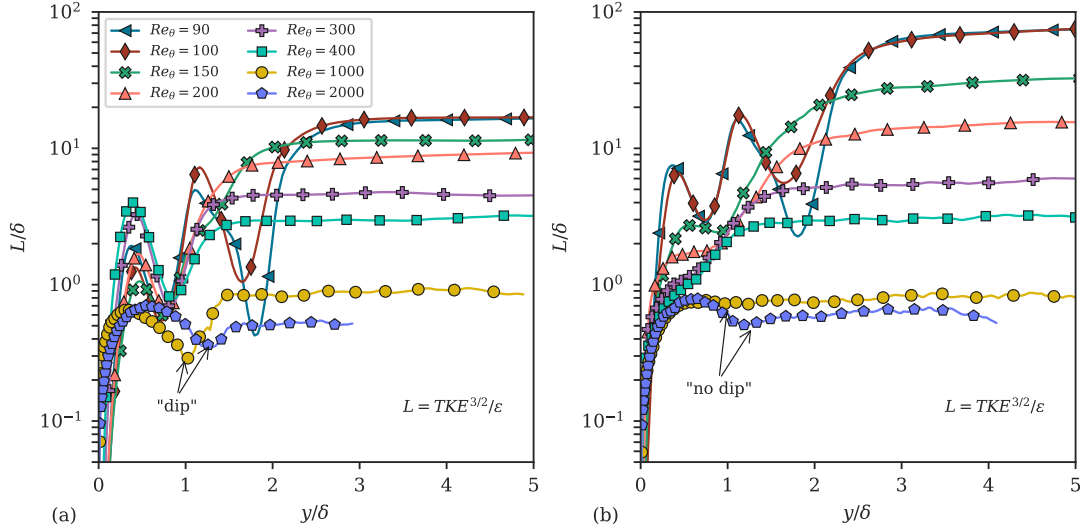


FIG. 9. Profiles of large-eddy scale L/δ before, during and after transition in (a) WM150 and (b) WM600.

(see Fig. 8). As Re_θ increases (moving downstream), there is a successive reduction in the large-eddy length scale relative to the local boundary-layer thickness. For WM150 case, in Fig. 9(a), there is a noticeable “dip” near the boundary-layer edge in the profiles of $Re_\theta = 1000$ and 2000 . We believe that the minima of such a “dip” corresponds to the boundary-layer turbulence and freestream turbulence interface (BTFTI) separating the two types of turbulent motions. Instantaneous BTFTIs of WM300 were studied in Wu et al. [29] using the probability density functions of passive scalar and vorticity. Fig. 9 provides a hint on a new indicator for locating the BTFTI. The absence of a “dip” in the WM600 profiles is consistent with the physical mechanisms that strong perturbations disturb the boundary layer underneath the FST. This interaction obscures the distinctions between the two turbulent regions, supporting our conjecture that beyond $FSTI_{in} \approx 6\%$, the boundary layer may get significantly affected by the freestream turbulence.

Fig. 10 presents the wall-normal profiles of the normalized Taylor-microscale (λ/δ) at eight selected streamwise stations for WM150 and WM600. Here $\lambda^2 = 2u_{rms}^2/(\partial u/\partial x)^2$. The freestream values of λ/δ decrease along the downstream direction, indicating that the freestream Taylor-microscale grows more slowly than the boundary layer. For the WM150 case, there is a noticeable “step” near the boundary-layer edge bridging the near-wall flow and the FST in both the turbulent region profiles of $Re_\theta = 1000$ and 2000 . We also consider these statistical markers of the BTFTI. Similarly, there is a lack of a “step” in Fig. 10(b) for the WM600 case at $Re_\theta = 1000$ and 2000 stations.

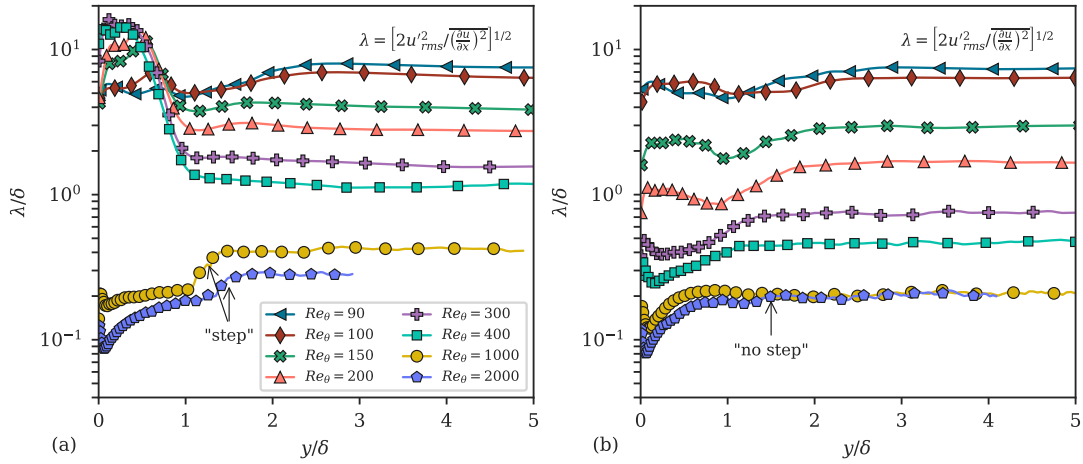


FIG. 10. Profiles of Taylor-microscale λ/δ before, during and after transition in (a) WM150 and (b) WM600.

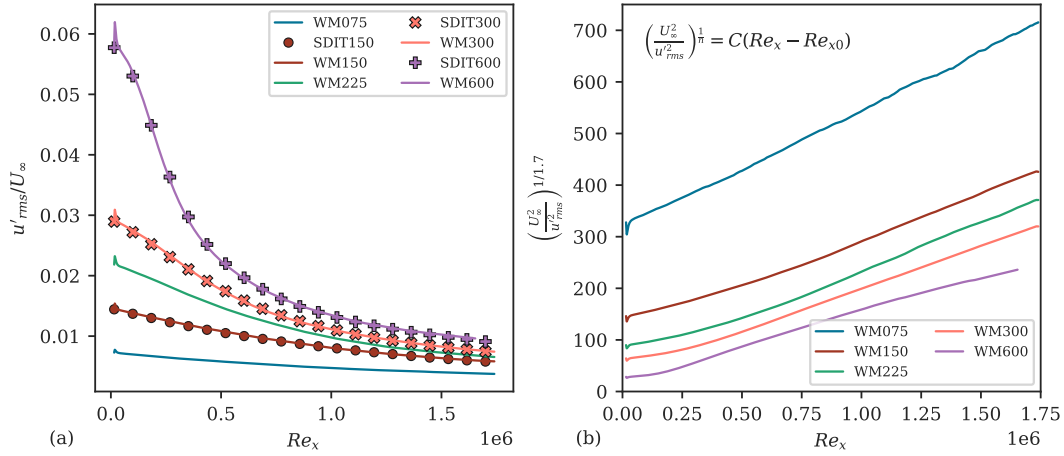


FIG. 11. (a) Decay of freestream turbulence intensity in the WM-series and the SDIT-series cases and (b) fitting of the freestream turbulence intensity decay into a power-law with exponent 1.7 in the WM-series.

IV. DECAY OF FREESTREAM TURBULENCE

In this section, we compare the streamwise developments of the turbulence intensities, viscous dissipation ε , large-eddy scale L , and Taylor-microscale λ for spatially developing isotropic turbulence and compare it to the corresponding freestream flow of a transitional boundary layer.

Fig. 11 presents the decay of u'_{rms}/U_∞ as a function of Re_x . For the WM-series, the u'_{rms} at each Re_x station is obtained by averaging the freestream values over the wall-normal range $500\theta_{in} < y < 800\theta_{in}$ (see Fig. 4). For the SDIT-series, the u'_{rms} is obtained by averaging the values over the wall-normal range $0.4L_y < y < 0.6L_y$ (see Fig. 5). The decay of turbulence intensity in the WM-series is nearly identical to the SDIT-series counterparts, implying that the presence of the wall (and the associated boundary layer) has a minimal effect on the rate of the FST decay. In Fig. 11(b), assuming a power-decay, $U_\infty^2/u'^2_{rms} = a(Re_x - Re_{x_0})^n$, we plot Re_x versus $(U_\infty^2/u'^2_{rms})^{1/n}$ to identify the exponent n where x_0 is an unknown virtual origin of the grid turbulence. For the WM075 flow, the entire streamwise growth is nearly linear. For the higher FST level flows, the linear region only appears for $Re_x > 1.0 \times 10^6$. The value of $n = 1.7$ is also consistent with the experiments of Ling and Wan [11] for isotropic turbulence.

Next, we assess the development of the turbulence length scales in the freestream region of the WM-series and SDIT-series flows. Fig. 12a compares the variations of λ/θ_{in} with Re_x between WM150 and SDIT150, and between WM600 and SDIT600. The freestream λ value is obtained from $y = 2\delta(x)$ location for the WM series. The Taylor-microscale

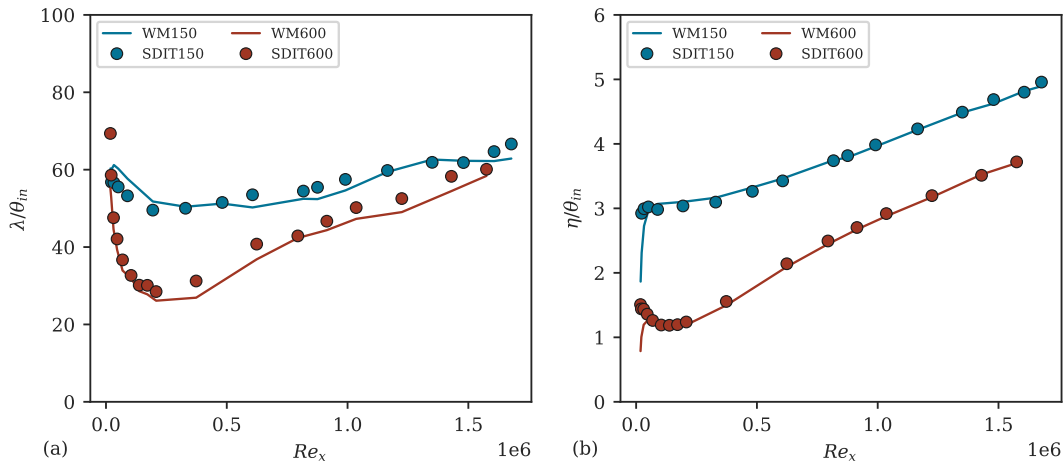


FIG. 12. Comparison of the freestream turbulence length scale variations in the WM-series and those in the SDIT-series. In the WM-series, data points are evaluated at $y = 2\delta(x)$. In the SDIT-series, data points are averaged over the wall-normal range $0.4L_y < y < 0.6L_y$. (a) Taylor-microscale; (b) Kolmogorov length scale.

for the WM-series flows develops similarly to their corresponding SDIT flows. Similarly, in Fig. 12b, we find that the Kolmogorov scales between the WM-series and SDIT-series flows also evolve similarly (the freestream Kolmogorov length scale value is also obtained from $y = 2\delta(x)$ for WM-series flows).

V. BLASIUS LAYER BREAKDOWN MECHANISMS AT INTERMEDIATE FSTI

Within the context of bypass transition in the narrow sense, the mechanism of breakdown of a perturbed Blasius layer is synonymous with the mechanism of the inception of the turbulent spot at the smallest Re_x , which is generally quasi-cyclic. We believe that the inception of additional turbulent spots within a cycle further downstream of the existing infant turbulent spot (closest to the inlet) may facilitate the growth of the turbulent region but may not be directly responsible for the Blasius layer breakdown.

In Subsection 1.2, we reviewed previous DNS work concerning the role of streak primary instability and secondary instability leading to the breakdown of the Blasius layer in boundary-layer bypass transition in the narrow sense. For instance, Jacobs and Durbin [8] found streak primary instability relevant to the breakdown, Brandt et al. [3] and Alarcón et al. [2] advocated the roles of streak primary and secondary instabilities. On the other hand, Ovchinnikov et al. [17] and Wu et al. [28] provided evidence that infant turbulent spots form upstream of streak primary instability, hence streaks are not responsible for the Blasius layer breakdown in their particular $FSTI_{in}$ cases. Wu [26] reconciled the differences and conjectured that streak primary and secondary instabilities are important for $FSTI_{in} \leq 2\%$, whereas the self-amplifying process of oblique vortex filaments interacting with a Δ -shaped low-speed patch underneath are important for $FSTI$ greater than 2.5%.

For the WM150 flow, Fig. 13 presents isosurfaces of swirling strength, as defined in Adrian [1], colored by y/δ , and blue-colored isosurfaces of low-speed fluid $u' = -0.1U_\infty$. The long streaks indicate primary instability, and the highlighted two symmetric vortex filaments wrapping around one streak correspond to the ‘varicose mode’ streak secondary instability. The structure subsequently evolves into an infant turbulent spot, with no other turbulent spots in this cycle at a smaller Re_x . Thus, this particular spot may be directly responsible for the breakdown of the Blasius layer within this cycle (movies for this flow can be found in Wu [26]).

Similarly, for WM300 flow, Fig. 14 presents a set of isosurfaces of swirling strength, colored by y/δ , and blue-colored isosurfaces of low-speed fluid $u = -0.1U_\infty$. As highlighted by the long arrow, at the instant $t = 98000\Delta t$, there are two oblique vortex filaments, each interacting with a Δ -shaped low-speed patch underneath. Subsequently, the structures evolve into an infant spot with no other upstream spots in this cycle. Long streaks appear only downstream of this infant turbulent spot, in agreement with the observation of Ovchinnikov et al. [17] at $FSTI_{in} > 6\%$. Streak instabilities are not found to cause the Blasius layer breakdown in this case; however, they may facilitate the spreading of turbulent regions (movies for this case can also be found in Wu [26]).

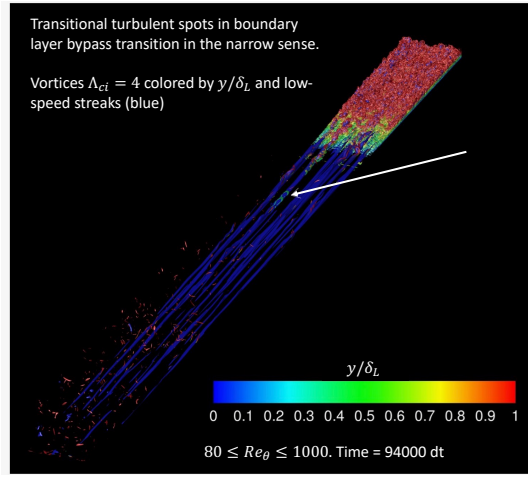


FIG. 13. Visualization of the inception of an infant turbulent spot in WM150 due to streak primary and secondary instabilities. Streaks are revealed using blue-colored iso-surfaces of $u' = -0.1U_\infty$. Vortices are revealed using iso-surfaces of swirling strength colored by $y/\delta(x)$.

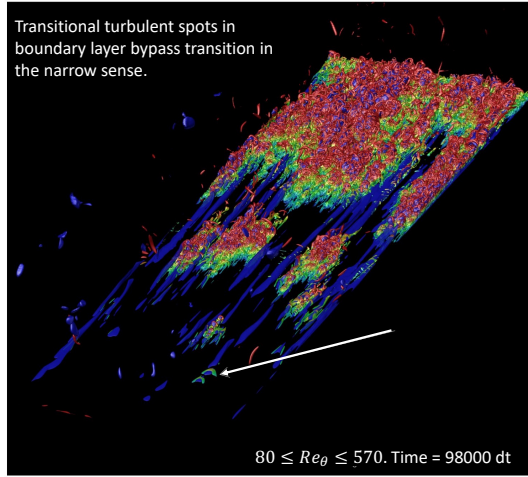


FIG. 14. Visualization of the inception of an infant turbulent spot in WM300. The process is not due to streak instabilities. Streaks are revealed using blue-colored iso-surfaces of $u' = -0.1U_\infty$. Vortices are revealed using iso-surfaces of swirling strength colored by $y/\delta(x)$.

Finally, for WM600 flow, Fig. 15 presents the isosurfaces of swirling strength, also colored by y/δ , and grey-colored isosurfaces of low-speed fluid $u = -0.2U_\infty$. At 6% FSTI, the transitional region is more chaotic than in other cases. As highlighted by a long arrow, at the instant $t = 60400\Delta t$, an oblique vortex filament interacts with a Δ -shaped low-speed patch underneath with no other spots further upstream. Subsequently, at $t = 60600\Delta t$, the structures evolve into an infant spot. Streaks appear downstream of this infant turbulent spot. Streak instabilities are not crucial in the inception of infant turbulent spots; however, they may aid in the growth of the turbulent region: when nearby existing turbulent spots interact with a streak, the streak may oscillate and break down. Supporting supplemental movies (WM600-Vortices, WM600-Streaks, and WM600-Streaks-and-Vortices) provide further evidence that at $FSTI_{in} = 6.0\%$, the breakdown is governed by the self-amplifying process of oblique vortex filaments interacting with a Δ -shaped low-speed patch underneath.

Wu [26] conjectured that the mechanism of self-amplifying oblique-vortex interaction with an underneath Δ -shaped low-speed patch is likely to be relevant at high inlet FST levels ranging from 2.5% to 6%. Observations in support of this conjecture include the WM300 and WM600 results and those of Ovchinnikov et al. [17]. Wu [26] also conjectured that it is quite likely that the streak-centered turbulent spot inception mechanism is relevant at $FSTI_{in}$ values ranging

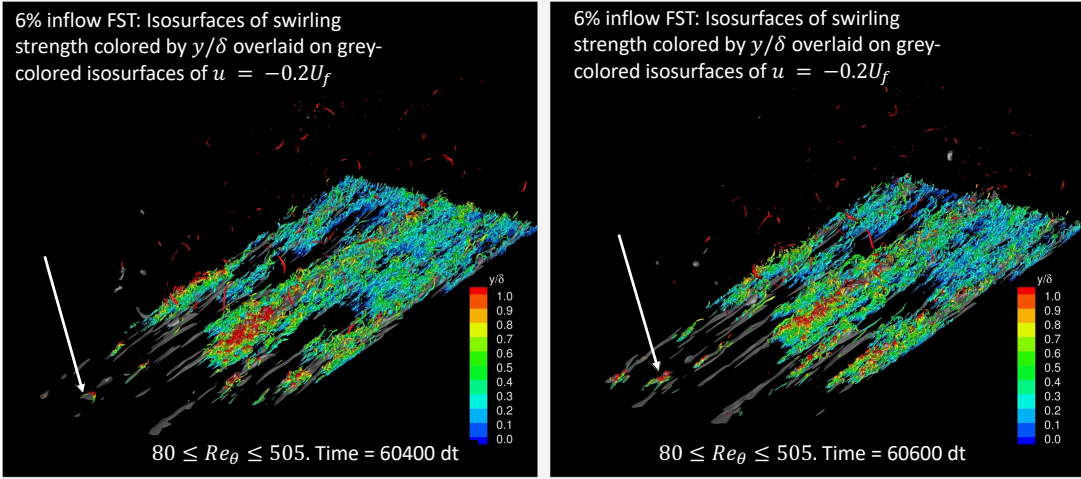


FIG. 15. Visualization of the inception of an infant turbulent spot in WM600. The process is not due to streak instabilities. Streaks are revealed using grey-colored iso-surfaces of $u' = -0.2U_\infty$. Vortices are revealed using iso-surfaces of swirling strength colored by $y/\delta(x)$.

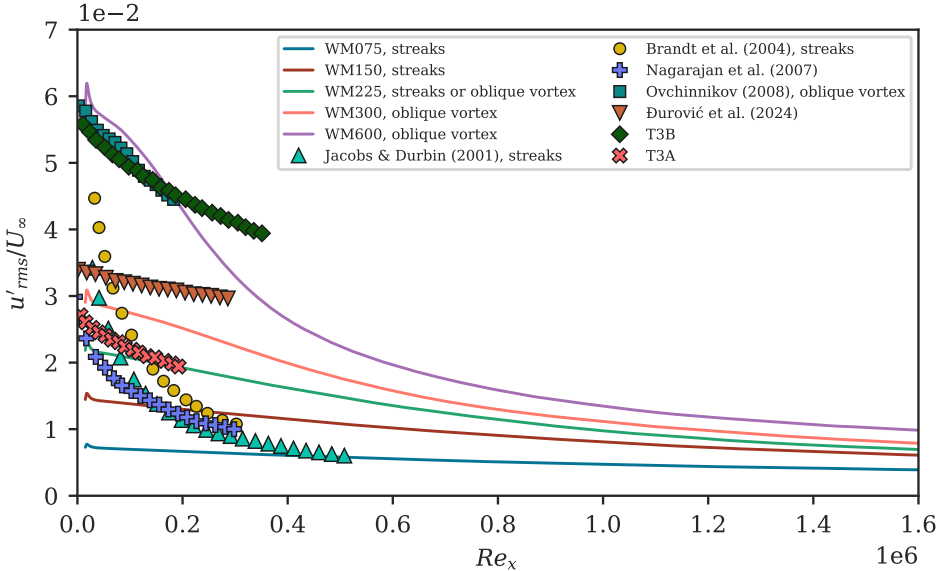


FIG. 16. Decay of freestream turbulence intensity in the present and previous studies on bypass transition in the narrow sense.

from 0.5% to 2%. The present WM150 results fall into this category. However, previous studies of Alarcón et al. [2], Brandt et al. [3], Jacobs and Durbin [8] reported that this streak-centered mechanism is still relevant even at their higher FSTI values of 3.5%, 3.45% and 4.7%, respectively. To reconcile this apparent contradiction, we refer the reader to Fig. 16. The FST introduced from the inlet in these simulations rapidly (for instance, compared to experiments of Roach [18]). The freestream turbulence intensity in Brandt et al. [3] is approximately 4.7% at the inlet but drops down to 1.2% by the station $Re_x = 2.5 \times 10^5$. Similarly, in Jacobs and Durbin [8], the FST decays from 3.5% at the inlet to 0.9% by the station $Re_x = 2.5 \times 10^5$. In contrast, the present DNS profiles show a slower decay than the existing DNS profiles. For example, in WM300, at $Re_x = 2.5 \times 10^5$, the $FSTI_{in} = 3.0\%$ case only decays to 2.5%. Thus, we conjecture that the bypass transition reported in these previous DNS might be occurring in a weaker FST environment than the reported corresponding $FSTI_{in}$, which would aid in reconciling the previous apparent contradiction. We briefly remark that, although, for Alarcón et al. [2] (who utilize the DNS of Đurović et al. [23]), at the station, $Re_x = 2.5 \times 10^5$, the freestream turbulence is higher than 3%, their C_f departs from the Blasius solution in the laminar region early, which is unexpected.

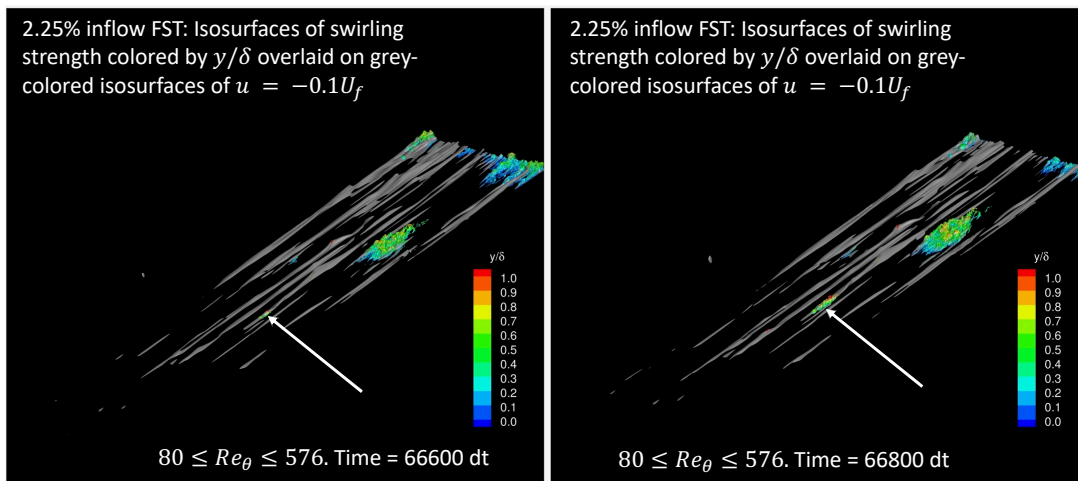


FIG. 17. Visualization of the inception of an infant turbulent spot in WM225 due to streak primary and secondary instabilities. Streaks are revealed using grey-colored iso-surfaces of $u' = -0.1U_\infty$. Vortices are revealed using iso-surfaces of swirling strength colored by $y/\delta(x)$.

Admitting the conjecture that the streak-centered turbulent spot inception mechanism is relevant at mild inlet FSTI levels ranging from 0.5% to 2%, and the mechanism of self-amplifying oblique-vortex interaction with an underneath Δ -shaped low-speed patch is relevant at stronger inlet FSTI levels ranging from 2.5% to 6%, we assess the intermediate zone between FSTI 2.0% and 2.5%. For instance, finding evidence of the co-existence of the two mechanisms in one flow at an intermediate FSTI would lend more support to our conjectures.

In this spirit, for WM225 flow, Fig. 17 presents, at two consecutive instants, iso-surfaces of the vortex identifier swirling strength, colored by y/δ , overlaid on the grey-colored iso-surfaces of low-speed fluid $u/U_\infty = -0.1$. Regular and long low-speed streaks are abundant. In the figure, at $t = 66600\Delta t$, symmetric boundary-layer vortex filaments (small hairpins) partially wrap the tail portion of one such streak. This results in the formation of an infant turbulent spot subsequently at $t = 66800\Delta t$ with no other spots further upstream in this cycle. The Blasius layer breakdown in this cycle is due to streak primary and secondary instabilities. For the same flow of WM225, at another two consecutive instants, Fig. 18 reveals the other breakdown mechanism. At $t = 65200\Delta t$, a pair of oblique vortex filaments flank a Δ -shaped low-speed patch underneath (in $y < 0.7\delta$). Note there is no turbulent spot upstream of this oblique vortex, and this structure is at the smallest Re_x in this cycle. Growth and amplification of the oblique vortex and the Δ -shaped low-speed patch can be seen at $t = 65400\Delta t$. The Blasius layer breakdown in this cycle is due to the oblique vortex mechanism, not streaks (full dynamic views of the two breakdown paths in the WM225 flow can be found in Supplemental Movies: WM225-Vortices, WM225-Streaks, and WM225-Streaks-and-Vortices. These three movies cover the transition stage and show the development history of boundary-layer vortices, low-speed structures, and vortices overlaid onto the low-speed structures, respectively).

Thus, we believe that there is sufficient evidence demonstrating the co-existence of the following two breakdown mechanisms in a given flow of the boundary-layer bypass transition at $FSTI_{in} = 2.25\%$: the mechanism of long low-speed streak primary instability followed by the ‘sinuous mode’ and ‘varicose mode’ secondary instability and the self-amplifying process of oblique vortex filaments interacting with a Δ -shaped low-speed patch underneath. Here, only the event of the inception of the one infant turbulent spot closest to the inlet in a cycle is considered instrumental in the laminar layer breakdown. Thus, at any instant, there can, at most, be only one breakdown mechanism at play. In this work, co-existence refers to both mechanisms being found in the same flow at different time instants.

VI. CONCLUDING REMARKS

This work provides a new database of comprehensive direct numerical simulation benchmarks of bypass transition. Detailed statistics and descriptions of the length-scales and dissipation are also provided for freestream turbulence intensity (FSTI) levels of 0.75%, 1.5%, 2.25%, 3.0%, 6.0%. We show that the presence of a wall (and the growing boundary layer) does not significantly affect the decay rates or the turbulence length scales (Taylor and Kolmogorov)

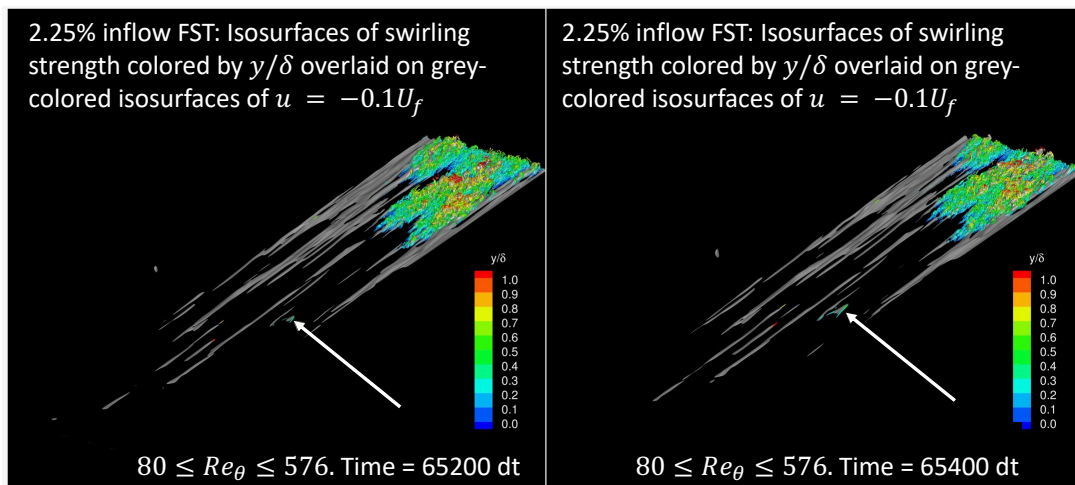


FIG. 18. Visualization of the inception of an infant turbulent spot in WM225 not due to streak instabilities. Streaks are revealed using grey-colored iso-surfaces of $u' = -0.1U_\infty$. Vortices are revealed using iso-surfaces of swirling strength colored by $y/\delta(x)$.

in the freestream flow compared to its spatially evolving homogeneous flow counterpart. Further, this study reveals important insights into the transition process across various FSTI levels. Specifically, at an intermediate FSTI equal to 2.25%, we provide evidence for the co-existence of two distinct breakdown mechanisms: the low-speed streak primary instability known to exist at low FSTI and the self-amplifying oblique vortex filaments known to exist at high FSTI. We also provide evidence that a reasonable upper limit for bypass transition in the narrow sense may be $FSTI \approx 6\%$.

ACKNOWLEDGEMENTS

This work was pursued during the 2024 Center for Turbulence Research Summer Program. X.W. is supported by the NSERC Discovery Grant and Digital Alliance Canada. C.A.G. and R.A. were supported by the NASA Transformational Tools and Technologies Program (grant #80NSSC20M0201). R.A. also acknowledges support from Boeing Research and Technology (grant #2024-UI-PA-100) and the Franklin P. and Caroline M. Johnson Fellowship at Stanford University. The authors gratefully acknowledge helpful discussions with Prof. Parviz Moin.

-
- [1] R. J. Adrian. Hairpin vortex organization in wall turbulence. *Physics of fluids*, 19(4), 2007.
 - [2] J. M. F. Alarcón, A. V. Cavalieri, A. Hanifi, and D. S. Henningson. Role of streak secondary instabilities on free-stream turbulence-induced transition. *Journal of Fluid Mechanics*, 988:A6, 2024.
 - [3] L. Brandt, P. Schlatter, and D. S. Henningson. Transition in boundary layers subject to free-stream turbulence. *Journal of Fluid Mechanics*, 517:167–198, 2004.
 - [4] P. Durbin. An intermittency model for bypass transition. *International Journal of Heat and Fluid Flow*, 36:1–6, 2012.
 - [5] J. H. Fransson and S. Shahinfar. On the effect of free-stream turbulence on boundary-layer transition. *Journal of Fluid Mechanics*, 899:A23, 2020.
 - [6] X. Ge, S. Arolla, and P. Durbin. A bypass transition model based on the intermittency function. *Flow, turbulence and combustion*, 93:37–61, 2014.
 - [7] C. A. Gonzalez, R. Agrawal, X. Wu, and P. Moin. Direct numerical simulation benchmarks for the prediction of boundary-layer bypass transition in the narrow sense. *Proceedings of the Summer Program, Center for Turbulence Research*, pages 3–12, 2024.
 - [8] R. Jacobs and P. Durbin. Simulations of bypass transition. *Journal of Fluid Mechanics*, 428:185–212, 2001.
 - [9] J. Kendall. Experiments on boundary-layer receptivity to freestream turbulence. In *36th AIAA Aerospace Sciences Meeting and Exhibit*, page 530, 1998.
 - [10] B. E. Launder and D. B. Spalding. The numerical computation of turbulent flows. In *Numerical prediction of flow, heat transfer, turbulence and combustion*, pages 96–116. Elsevier, 1983.

- [11] S. Ling and C. Wan. Decay of isotropic turbulence generated by a mechanically agitated grid. *The Physics of Fluids*, 15(8):1363–1369, 1972.
- [12] M. Matsubara and P. H. Alfredsson. Disturbance growth in boundary layers subjected to free-stream turbulence. *Journal of Fluid Mechanics*, 430:149–168, 2001.
- [13] B. J. McKeon, J.-d. Li, W. Jiang, J. F. Morrison, and A. J. Smits. Further observations on the mean velocity distribution in fully developed pipe flow. *Journal of Fluid Mechanics*, 501:135–147, 2004.
- [14] F. R. Menter, R. Langtry, and S. Völker. Transition modelling for general purpose CFD codes. *Flow, turbulence and combustion*, 77:277–303, 2006.
- [15] F. R. Menter, P. E. Smirnov, T. Liu, and R. Avancha. A one-equation local correlation-based transition model. *Flow, Turbulence and Combustion*, 95:583–619, 2015.
- [16] S. Nagarajan, S. Lele, and J. Ferziger. Leading-edge effects in bypass transition. *Journal of Fluid Mechanics*, 572:471–504, 2007.
- [17] V. Ovchinnikov, M. M. Choudhari, and U. Piomelli. Numerical simulations of boundary-layer bypass transition due to high-amplitude free-stream turbulence. *Journal of Fluid Mechanics*, 613:135–169, 2008.
- [18] B. D. Roach, PE. The influence of a turbulent freestream on zero pressure gradient transitional boundary layer development, Part I: Test cases T3A and T3B. *Numerical Simulation of Unsteady Flows and Transition to Turbulence*, eds Pironneau O, Rodi W, Ryhming IL, Savill AM, Truong TV (Cambridge Univ Press, Cambridge, UK, pages 319–347, 1990.
- [19] T. H. Shih, W. W. Liou, C. S. Pyo, and W. D. Roquemore. A realizable k- ϵ turbulence model for complex flows. *Computers & Fluids*, 24(3):227–238, 1995. doi:10.1016/0045-7930(94)00032-5.
- [20] Y. Suzen and P. Huang. Modeling of flow transition using an intermittency transport equation. *Journal of Fluids Engineering*, 122(2):273–284, 2000.
- [21] J. D. Swearingen and R. F. Blackwelder. The growth and breakdown of streamwise vortices in the presence of a wall. *Journal of Fluid Mechanics*, 182:255–290, 1987.
- [22] H. Tennekes and J. L. Lumley. *A first course in turbulence*. MIT press, 1972.
- [23] K. Đurović, A. Hanifi, P. Schlatter, K. Sasaki, and D. S. Henningson. Direct numerical simulation of transition under free-stream turbulence and the influence of large integral length scales. *Physics of Fluids*, 36(7), 2024.
- [24] K. Westin and R. Henkes. Application of turbulence models to bypass transition. *Journal of Fluids Engineering*, 1997.
- [25] K. Westin, A. Boiko, B. Klingmann, V. Kozlov, and P. Alfredsson. Experiments in a boundary layer subjected to free stream turbulence. part 1. boundary layer structure and receptivity. *Journal of Fluid Mechanics*, 281:193–218, 1994.
- [26] X. Wu. New insights into turbulent spots. *Annual Review of Fluid Mechanics*, 55(1):45–75, 2023.
- [27] X. Wu, R. G. Jacobs, J. C. Hunt, and P. A. Durbin. Simulation of boundary layer transition induced by periodically passing wakes. *Journal of Fluid Mechanics*, 398:109–153, 1999.
- [28] X. Wu, P. Moin, J. M. Wallace, J. Skarda, A. Lozano-Durán, and J.-P. Hickey. Transitional–turbulent spots and turbulent–turbulent spots in boundary layers. *Proceedings of the National Academy of Sciences*, 114(27):E5292–E5299, 2017.
- [29] X. Wu, J. M. Wallace, and J.-P. Hickey. Boundary layer turbulence and freestream turbulence interface, turbulent spot and freestream turbulence interface, laminar boundary layer and freestream turbulence interface. *Physics of Fluids*, 31(4), 2019.